Heptad-Repeat Regions of Respiratory Syncytial Virus F_1 Protein Form a Six-Membered Coiled-Coil Complex

Mary K. Lawless-Delmedico,* Prakash Sista, Ratna Sen, Nicole C. Moore, James B. Antczak,‡ Jonathan M. White, Reagan J. Greene, Karen C. Leanza, Thomas J. Matthews, and Dennis M. Lambert

Trimeris, Inc., 4727 University Drive, Durham, North Carolina 27707

Received March 1, 2000; Revised Manuscript Received June 9, 2000

ABSTRACT: The Respiratory Syncytial Virus (RSV) fusogenic glycoprotein F_1 was characterized using biochemical and biophysical techniques. Two heptad-repeat (HR) regions within F_1 were shown to interact. Proteinase-K digestion experiments highlight the HR1 region (located proximal to the fusion peptide sequence) of the F_1 protein to which an HR2-derived (located proximal to the membrane-spanning domain) peptide binds, thus protecting both the protein and peptide from digestion. Solution-phase analysis of HR1-derived peptides shows that these peptides adopt helical secondary structure as measured by circular dichroism. Sedimentation equilibrium studies indicate that these HR1 peptides self-associate in a monomer/trimer equilibrium with an association constant of $5.2 \times 10^8\ M^{-2}$. In contrast, HR2-derived peptides form random monomers in solution. CD analysis of mixtures containing peptides from the two regions demonstrate their propensity to interact and form a very stable (T_m = 87 °C), helical (86% helicity) complex comprised of three HR1 and three HR2 members.

Respiratory syncytial virus (RSV)[1] is a member of the pneumovirus group in the *Paramyxoviridae* family, and the primary cause of lower respiratory infection and pneumonia in infants, young children, bone marrow transplant patients, the elderly, and other immunocompromised individuals (*1*, *2*). RSV is an enveloped virus which contains two major surface glycoproteins: a receptor binding protein (G) which facilitates attachment to cells, and a fusion protein (F) (*3*, *4*). The RSV−F protein is a class I integral membrane protein which is comprised of two subunits, F_1 and F_2, which are linked by a single disulfide bridge (see Figure 1A). F_1 anchors the protein in the viral membrane via a hydrophobic sequence ("transmembrane anchor"). Another hydrophobic sequence located at the amino terminus of F_1 serves as the "fusion peptide" domain which anchors the fusion protein into the target cell membrane during the membrane fusion process (*5*−*7*).

Membrane fusion is an essential step in the life cycle of enveloped viruses; it allows the viral contents to be deposited into the cytoplasm and is followed by subsequent production of infectious virions (*5*−*7*). Fusion begins after the virus binds to the target cell, through an association of a viral attachment protein with the appropriate cellular receptor(s). This attachment is followed by conformational changes of the viral fusion protein which disrupt the target cell membrane, permitting the viral and cellular membranes to coalesce, allowing viral entry. These conformational changes of the viral fusion protein involve exposure and insertion of the hydrophobic F_1 amino-terminus into the target cell membrane, juxtaposition of the two membranes, and creation of a fusion pore. At least two conformational states are proposed to exist: the native state, in which the fusion peptide is masked until the target cell is bound, and the fusogenic state, in which the fusion peptide has been inserted into the target membrane.

Structural studies on viral fusion proteins and peptides derived from their subdomains have demonstrated the importance of the coiled-coil motif in the native and fusogenic states of Influenza (*8*−*10*), Human Immunodeficiency Virus (HIV) (*11*−*14*), Simian Immunodeficiency Virus (SIV) (*15*−*18*), Ebola (*19*, *20*), Moloney murine leukemia virus (MuLV) (*21*), and Simian Virus 5 (SV5) (*22*, *23*). Earlier identification of heptad-repeat regions within the ectodomains of viral fusion proteins had implicated coiled-coil motifs in the structure of these proteins (*8*, *24*−*28*). A heptad repeat (HR) is defined by hydrophobic residues appearing at *a* and *d* positions of a sequence designated *abcdefg*. This primary sequence has been shown to have the propensity to fold into coiled-coils, in which two or more α-helices wind around each other, forming a supercoil (*29*, *30*). The fusion proteins of enveloped viruses contain at least two heptad-repeat regions: one located proximal to the fusion peptide (HR1, see Figure 1A) and one located close to the membrane (HR2). Crystallographic studies implicate a common structural motif adopted by these two HR regions: a central trimeric coiled-coil formed by the interaction of three HR1 domains and three HR2 domains aligned in an antiparallel fashion along the grooves located between the helices of the central HR1 coiled-coil (*9*, *12*−*15*, *17*, *19*, *20*, *23*). Thus, a six-membered coiled-coil is formed.

* To whom correspondence should be addressed. Phone: (919) 408-5128. Fax: (919) 408-5191. E-mail: mdelmedico@trimeris.com.

‡ Present Address: Cogent Neuroscience, Inc., 710 West Main St., Durham, NC 27701.

[1] Abbreviations: RSV, respiratory syncytial virus; HR1, heptad-repeat region 1; HR2, heptad-repeat region 2; HIV, Human Immunodeficiency Virus; HPIV-3, Human Parainfluenza Virus Type 3; CD, circular dichroism; M_w, weight-averaged molecular weight.

10.1021/bi000471y CCC: $19.00
Published on Web 08/25/2000

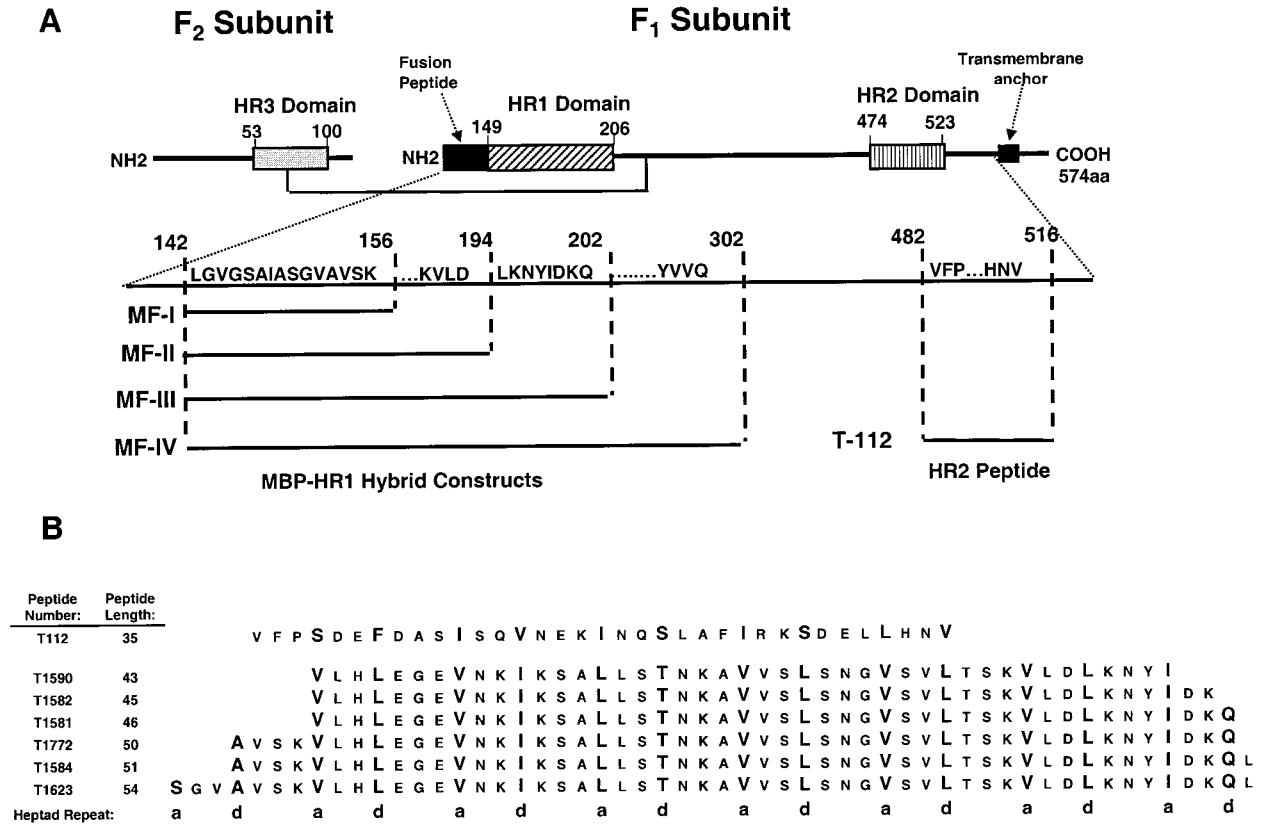

FIGURE 1: Protein and peptide reagents used in this study. (A) Schematic of the ectodomain of the RSV F_1 and F_2 subunits, illustrating the relative positions of the heptad-repeat regions 1 (diagonal stripe), 2 (vertical stripe), and 3 (gray). Recombinant proteins MF−I, MF−II, MF−III, and MF−IV used herein are derived from the HR1 region; the peptide T-112 is derived from the HR2 region. Numbering of amino acids follows Collins et al. (*54*). (B) Sequences of synthetic peptides. All peptides have blocked amino and carboxy terminii.

In the case of HIV-1, Wild et al. demonstrated that synthetic peptides derived from each of these potentially helical regions within the transmembrane protein gp41 were potent inhibitors of viral fusion and infection (*31*−*33*). Our laboratory reported that HR2-derived peptides from the paramyxoviruses RSV, Human Parainfluenza Virus Type-3 (HPIV-3), and measles (MV) exhibit specific and selective antifusion and antiviral activity (*34*). Similar antiviral peptides derived from heptad-repeat regions contained in the fusion proteins of HPIV-3, HPIV-2, Feline Immunodeficiency Virus (FIV), Newcastle Disease Virus (NDV), and Sendai virus have been identified (*35*−*38*). Previous studies in HIV-1 and NDV have suggested a mechanism of action for these antiviral peptides based on a high affinity association between peptide and protein models of the two heptad-repeat domains (*39*−*43*). This mechanism of action for HIV-1 was reinforced by genetic studies that clearly mapped resistance for HR2-derived peptides to the HR1 domain (*44*). The related mechanistic models were further solidified and structural details of the complexes elucidated by X-ray crystallographic analysis of the HIV-1 HR1/HR2 core (*12*−*14*). A recent report has demonstrated similar crystallographic evidence for HR1/HR2 binding interactions within the F protein of the paramyxovirus SV5 (*23*).

Previous work in our laboratory identified two heptad-repeat regions of the RSV F_1 subunit and a third heptad-repeat region (designated HR3, see Figure 1A) in the F_2 subunit (*34*). Peptides from the HR2 region showed potent, specific anti-viral activity, presumably by inhibiting the viral fusion process. By analogy to the HIV system, it is reasonable to speculate that the target of these anti-viral peptides could be the HR1 region of the F_1 protein. The goals of the present study are to identify the target HR1 binding region on the RSV−F_1 protein and to characterize the interaction between the two heptad-repeat regions in the solution phase. We have simplified this approach through the use of synthetic peptides derived from the HR2 region. The HR1 target region is represented by recombinant protein constructs which include varying lengths of the RSV−F_1 protein. These studies are essential for drug discovery efforts in this important therapeutic area. Inhibition of the HR1−HR2 interaction in HIV-1 gp41 has been demonstrated as a viable therapeutic target (*45*). An understanding of the solution-phase HR1−HR2 interactions is essential both in designing molecular screens to discover inhibitory agents and in laying the groundwork for crystallographic analysis of this protein−protein interaction.

MATERIALS AND METHODS

*Cloning and Expression of Recombinant RSV F_1 Constructs.*The full-length RSV F protein gene cDNA was cloned by standard recombinant techniques (J. Antczak, unpublished) using a recombinant vaccinia virus containing the RSV (strain A2) F protein gene (a gift from Dr. Peter Collins) as a PCR template (*46*). The entire F protein gene (clone F0 AA1−574 of the F protein) and a truncated version F1ΔHR2/FP (AA 142−485) were initially cloned into the pFLAG-ATS vector (IBI−Kodak) and then subsequently recloned into the pMAL c2 vector (New England Biolabs, Boston, MA) to generate hybrids with the *Escherichia coli* (*E. coli*) maltose binding protein (MBP). Thereafter, specific PCR primers were designed such that they contained restriction

sites permitting in-frame hybrids between MBP and RSV F protein-gene truncations depicted in Figure 1A [sense primer, 5′-GGA AGG AAT TCC CGG TTA GG-3′ (TO-223); antisense primer, for MF−IV, 5′-TGC TCT AGA CTA TTG TAC TAC ATA TGC-3′ (TO-225); for MF−III, 5′-TGC TCT AGA CTA CTT AGA TAC AGC AAC G-3′ (TO-229); for MF−II, 5′-TGC TCT AGA CTA TTG TTT ATC TAT ATA GTT TTT-3′ (TO-383); and for MF−I, 5′-TGC TCT AGA CTA GTC TAA CAC TTT GCT GG-3′ (TO-384)]. The primers were used in PCR reactions with the F1ΔHR2/FP (pJAMCF4.C12) recombinant clone as template. The PCR products were purified and ligated into pMAL-c2 vector and transformed into *E. coli*. Resulting recombinants were verified by sequence analysis. Recombinant protein was expressed in culture and biochemically purified by affinity chromatography using an amylose resin as recommended by New England Biolabs.

Proteinase-K Protection Experiments. A total of 60 μg each of the various RSV−F_1 constructs were incubated for 1 h at room temperature with or without 4 μg of T-112 peptide in 80 μL of final reaction volume containing 10 mM Tris (hydroxymethyl) aminomethane (TRIS, Sigma, St. Louis, MO), 200 mM sodium chloride (Sigma, St. Louis, MO), 50 mM maltose (Fisher, Pittsburgh, PA), and 1 mM EDTA (Fisher, Pittsburgh, PA), at pH 7.4. Mixtures were treated with 5 μg/mL proteinase-K (Sigma, St. Louis, MO) or an equivalent volume of buffer, vortexed, then incubated 1 h at 37 °C. Phenylmethanesulfonyl fluoride (PMSF, Boehringer Mannheim, Indianapolis, IN) was added to achieve a 2 mM final concentration to stop proteolytic digestion. A total of 20 μL of each sample was removed and added to 10 μL of a sample buffer (NE Biolabs, Boston, MA) containing 6 w/v% sodium dodecyl sulfate, DTT, 187.5 mM TRIS, 30% glycerol, and bromophenol blue. The mixtures were heated 5 min at 90 °C. A total of 15 μL of the samples was run on a 10−20% tricine polyacrylamide gel (Novex, San Diego, CA), stained with Coomassie brilliant blue and destained with a 10% methanol−10% acetic acid (Fisher, Norcross, GA) mixture. All proteins were treated identically, except that the MF−II samples were lyophilized after the addition of PMSF and resuspended in a smaller volume to achieve solute concentrations comparable to the other three constructs. Treatment of the other constructs in this manner produced results identical to those reported. N-Terminal sequencing was performed by Argo BioAnalytical Inc. (Morris Plains, NJ).

Peptide Synthesis and Purification. Peptide synthesis was performed on a Rainin Symphony multiplex peptide synthesizer (Rainin Instrument Company, Woburn, MA) using 9-fluorenylmethoxycarbonyl (FMOC) chemistry protocols (*47*, *48*). Peptides were synthesized on Rink Amide MBHA resin (0.40 mequiv, Peptides International, Louisville, KY) for C-terminal amides and acetylated on the N-terminus using acetic anhydride (Mallinckrodt Baker Inc., Phillipsburg, NJ) and NMM in DMF (1:1:20 v/v). FMOC amino acids (10 equiv, Rainin Instrument Comp., Chem Impex International, Peptides International and Genzyme Pharmaceuticals, Cambridge, MA) were activated in situ using 1-hydroxybenzotriazole (HOBt, Chem Impex International), *O*-(benzotriazol-1-yl)-*N*,*N*,*N*′,*N*′-tetramethyluronium hexafluorophosphate (HBTU, Quantum Biotechnologies, Montreal, Qc, Canada) and *N*-methylmorpholine (NMM, Chem Impex International) with coupling reactions proceeding for 30 min. For some residues (arginine, asparagine, glutamine, histidine, tryptophan, and proline), double coupling reactions were routinely performed. Removal of the FMOC group was performed using 20% Piperidine (PIP, Chem Impex International, Wood Dale, IL.) in dimethylformamide (DMF, Allied/Burdick and Jackson, Muskegon, MI) with the residual PIP being removed by three consecutive DMF washes. Peptide cleavage from the resin support was performed using 90% trifluoroacetic acid (TFA), 5% dithiothreitol (DTT), and 5% water (10 mL/400 mg of resin) for 2 h at room temperature, followed by precipitation in cold ethyl ether. The precipitated peptide was centrifuged to pellet (1250g for 5 min, Jouan, Inc., Winchester, VA) and washed three times with ethyl ether. Peptide pellets were dried under vacuum and redissolved in 50% acetonitrile (ACN, Allied/Burdick and Jackson). Peptides were analyzed and purified by reversed-phase high-performance liquid chromatography (RP-HPLC) on a C-8 column (Vydac C-8, 4.6 × 250 mm or 5.0 × 25 cm, Vydac Separations Group, Hesperia, CA) using an ACN/water/TFA buffer system (buffer A, 0.1% TFA in water; buffer B, 0.1% TFA in ACN). Analytical HPLC absorbance profiles at 220-nm were obtained on a Rainin/Varian analytical system using a 30−60% B over 30 min at 1.0 mL/min. The purification of peptides was performed on a Waters Prep 4000 or Rainin/Varian SD-1 Prep system using a gradient of 30 to 60% B over 60 min at 50 or 60 mL/min, respectively. Fractions were collected and analyzed as previously mentioned and pooled to obtain peptides that were >95% pure. The pooled effluent was lyophilyzed and dried peptide stored at 4 or −20 °C with desiccant. Peptide identity was confirmed with electrospray mass spectrometry (Finnigan LCQ).

Peptide content was determined by amino acid analysis performed at the University of Michigan, Protein & Carbohydrate Structure Facility (Ann Arbor, MI). Peptide solutions were prepared with PBS buffer containing 100 mM NaCl (Sigma, St. Louis, MO) and 50 mM sodium phosphate (Sigma, St. Louis, MO) adjusted to pH 7. Peptide concentrations were determined by one of two methods: either based on weight and volume, corrected for peptide content or by direct amino acid analysis of the prepared stock solutions (Biosynthesis, Inc., Lewisville, TX). Dilution of the stock solutions to final concentrations as noted in the text were performed in PBS.

Circular Dichroism Spectroscopy. Circular dichroism (CD) spectra were obtained using an AVIV Associates 62DS spectrometer equipped with a thermoelectric temperature controller. Spectra were obtained in 0.1, 0.5, and 1.0 cm quartz cells at 1 °C with 0.5 nm steps from 200 to 260 nm, 1.5 nm bandwidth, and an averaging time of 4 s/step. After the cell/buffer blank was subtracted, spectra were smoothed using a third-order least-squares polynomial fit with a conservative (5−10 point) window size to give random residuals. Mixing experiments were performed by comparing the spectrum of the two peptides mixed together in a 0.1 cm path length cell at the desired concentrations (*experimental*) to the sum of the individual spectra of the peptides, each solution in a 0.1 cm path-length cell (*model for no interaction*). Raw ellipticity values were converted to mean residue ellipticity using standard methods (*49*); the conversions for the mixing experiment spectra were performed using a

peptide length corresponding to the average of the two peptides. Thermal stability measurements were performed in 2 °C steps, with 1 min equilibration times. Spectra were smoothed, converted to mean residue ellipticity, and the corresponding value at 222 nm noted from each spectrum. The midpoints of the thermal melting transitions were taken to be the temperature at which the ellipticity value (at 222 nm) corresponded to half of the difference between the ellipticity value obtained 1 °C and the ellipticity value of the final, fully denatured sample. Percent helicity values were calculated using single value decomposition with a basis set of 33 protein spectra (*50*).

Analytical Ultracentrifugation. Sedimentation equilibrium experiments were performed on a Beckman Optima XL-A analytical ultracentrifuge at 4 °C. Six-channel cells (12 mm optical path length) were used with an An-60 Ti rotor operated at 13 500, 16 000, 17 000, 20 000, 21 000, 24 000, 25 000, 27 500, 30 000, and 35 000 rpm. The cell radii were scanned using 0.001 cm steps with 10 averages/scan. Data were analyzed using Beckman XLA data analysis software (version 3.01 for Windows) and Beckman-Origin software (version 3.78 for Windows). The methods described by Laue et al. were used to calculate partial specific volumes (v-bar, mL/g: T-1581 = 0.7539; T-1582 = 0.7574; T-1772 = 0.7546; T-1584 = 0.7574; T-1623 = 0.7557; T-112 = 0.7230) and the solvent density (ρ = 1.00895) at 4 °C (*51*). For peptide mixtures, a concentration-weighted average v-bar was used (for T1772:T112 ratios: v-bar = 0.7388 for 50:50 μM; 0.7493 for 50:10 μM; 0.7335 for 50:100 μM). The partial specific volumes were held constant for all models considered.

Single data files were normalized to 270 nm absorbance values using Beer's law. The data obtained with solutions containing the HR1 peptides were then analyzed using a single ideal species model to determine a weight-averaged molecular weight (M_w). Diagnostic plots of M_w/M_{w0} vs rpm/rpm$_0$ and M_w vs radial concentration were used to test for sample homogeneity (*52*−*54*). When systematic residuals or a M_w higher than the monomer molecular weight indicated the presence of self-association, associative models, such as monomer/trimer, monomer/tetramer, and monomer/dimer/tetramer were investigated. The suitability of a particular model (goodness of fit) was judged by the trends observed in the residuals (*55*). Using the associative model which produced random residuals when fitting individual data files, a simultaneous, global, weighted-fit of multiple data files (up to nine files with different concentrations and speeds) was performed (Beckman-Origin software) to determine the association constant and 95% confidence intervals. To convert the resulting association constant from absorbance units to concentration units, it was assumed that the absorbance of the *n*-mer is *n* times that of the monomer.

The data obtained with HR1−HR2 peptide mixtures were first analyzed with a single ideal species model. When a systematic trend in residuals coupled with the M_w not equal to a precise multimer of HR1 + HR2 was obtained, an alternate fitting scheme was explored. For this approach, we assumed that the solution contained fully associated HR1−HR2 complexes and unassociated HR1 and HR2 peptides. The mixtures were analyzed with a two-ideal species model, choosing one species to have a molecular weight of either 28 269 (corresponding to three HR1 plus three HR2 peptides) or 37 692 (corresponding to four HR1 plus four HR2 peptides). The other ideal species was taken to be 8400, the average molecular weight of the HR1 peptide T-1772 (12 797, see results) and HR2 peptide (4030).

RESULTS

Proteinase-K Protection Experiments Identify the HR1 Binding Region of the HR2 Peptide. To begin our study of the HR1−HR2 interactions in the RSV F_1 protein, several chimeric proteins were prepared in which the amino terminus of different portions of the F_1 ectodomain were linked to the carboxy terminus of *E. coli* maltose binding protein (MBP). Figure 1A presents the amino and carboxy termini of the F_1 portions of the chimera sequences; each of these proteins lack the amino terminal hydrophobic fusion peptide and include increasing lengths of F_1. The full F_1 sequence of RSV, strain A2, can be found in Collins et al., whose numbering scheme is followed herein (*56*). The protein MF−I includes residues 142−156 which immediately follow the fusion peptide sequence. MF−II includes residues 142−194, MF−III includes residues 142−202, and MF−IV includes residues 142−302. The latter three proteins include either portions (MF−II, MF−III) or the complete (MF−IV) region previously identified as heptad-repeat 1 (*34*). This region, designated HR1, is analogous to other viral systems which have such heptad-repeat regions proximal to the fusion peptide sequence.

To identify the HR1 region of RSV−F_1 to which the HR2-region peptide binds, limited proteolysis experiments were performed. These experiments used the HR2 peptide T-112 which bound to and protected the HR1 proteins from proteolytic digestion (see below). Similar protection was not observed for two other 35-residue peptides derived from the HR2 region which were shifted by five residues to the amino terminus and seven residues to the carboxy terminus, respectively (N. Moore, unpublished). Therefore, our work focused on the use of T-112 as our HR2-domain model peptide (see Figure 1B for sequence).

Figure 2A presents the SDS−PAGE results of an experiment in which binding of an HR2 peptide T-112 to the MF−IV protein protects both the peptide and a portion of MF−IV from proteolytic digestion. Nondigested MF−IV is shown in lane 2 with the major component at approximately 60 000 apparent molecular weight (theoretical molecular weight = 60 524). Treatment of MF−IV alone with proteinase-K (lane 3) yields two doublet bands at approximately 40 and 20 kDa. These bands appear to be derived from the MBP portion of the fusion protein since the same pattern was observed upon protease digestion of MBP (data not shown). Nondigested T-112 peptide is shown in lane 4; treatment of the peptide with proteinase-K (lane 5) digests the peptide into species which are too small to be detected on this gel. Lane 6 presents the mixture of MF−IV with T-112. Comparison of the proteinase-K treated mixture of MF−IV and T-112 (lane 7) with the proteinase-K treated protein MF−IV (lane 3) and peptide T-112 (lane 5) reveals two short fragments which are only apparent following digestion of the mixture of T-112 and MF−IV. One band is coincident with the native T-112 (sequence molar mass = 4030) and a second band of approximately 4500 appears as well. N-terminal sequencing of the second fragment reveals the sequence "VLHLE",

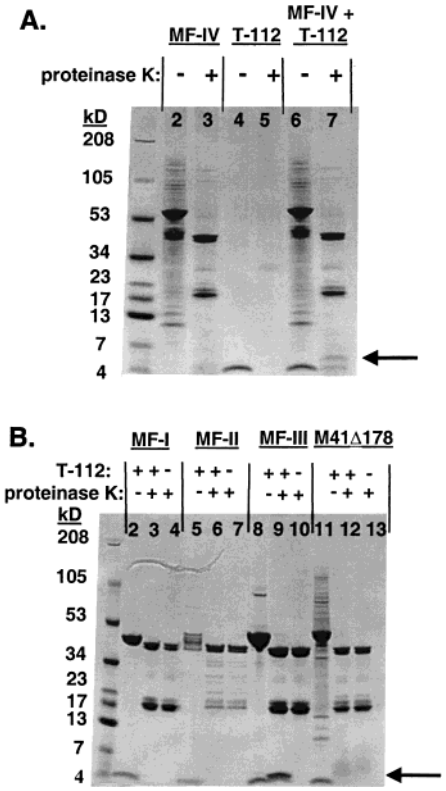

FIGURE 2: SDS−PAGE results for proteinase-K treatment of RSV−F_1 protein constructs, the HR2-derived peptide T-112, and mixtures thereof.

which is found in the amino terminal region of the F_1-protein and within the region identified as HR1.

Figure 2B presents the next series of experiments which identify the approximate C-terminus of HR1 required for binding of the HR2 peptide. Proteinase-K protection experiments identical to those described above were done using the shorter protein constructs, corresponding to different lengths of the F_1-protein (Figure 1A). The constructs MF−I and MF−II show no protection from proteinase-K digestion as a result of mixing with T-112 (lane 3 vs 4 and lane 6 vs 7, respectively). However, the construct MF−III shows protection from proteinase-K digestion (lane 9 vs 10) due to the presence of T-112, similar to that observed with the longer MF−IV protein. It is interesting to note that the MF−III protected fragment is visibly shorter (~4150 Da) than that produced by the longer MF−IV construct (~4500 Da). Taken together, these data suggest that the minimal C-terminal end of the HR1 target region required for HR2-binding is within the sequence "LKNYIDKQ". As a control for nonspecific binding, comparison of lanes 12 and 13 demonstrate that the T-112 peptide does not bind to an MBP fusion protein containing the ectodomain of the HIV-1 fusion protein gp41 (*39*), as no protease-protected fragment is observed in the presence of T-112.

Figure 1B presents the sequences of HR1 peptides synthetically prepared to examine the heptad-repeat domain interactions of the RSV F_1-protein. Peptide T-112 is derived from the HR2 region. The remaining six peptides represent different lengths of the HR1 region identified by the SDS−PAGE experiments. Peptide T-1582 has the exact N-terminal sequence which was identified from the proteinase-K experiments on MF−IV and the C-terminal sequence suggested

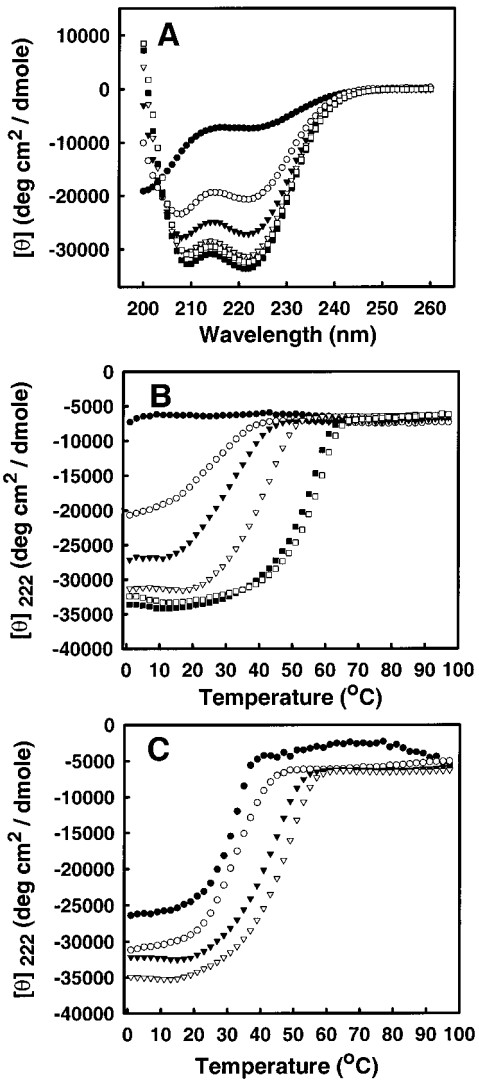

FIGURE 3: Circular dichroism spectra and thermal stability results for HR1 peptides in PBS pH 7. (A) CD spectra (mean residue ellipticity) of 35 μM solutions for T1590 (●), T-1582 (○), T-1581 (▼), T-1772 (▽), T-1584 (■), and T-1623 (□). (B) Mean residue ellipticity at 222 nm as a function of temperature for 35 μM solutions of T-1590 (●), T-1582 (○), T-1581 (▼), T-1772 (▽), T-1584 (■), and T-1623 (□). (C) Mean residue ellipticity at 222 nm as a function of temperature for increasing concentrations of T-1772: 1 μM (●), 10 μM (○), 50 μM (▼), and 100 μM (▽).

by the proteinase-K experiments on MF−II vs MF−III. Peptide T-1590 is two residues shorter than T-1582, while the remaining peptides, T-1581, T-1772, T-1584, and T-1623 are longer than T-1582, as depicted in Figure 1B.

CD Studies of HR1 Peptides Suggest Helical Self-Association. The solution-phase secondary structures of these peptides were examined using CD spectroscopy. Figure 3A presents the normalized CD spectra (mean residue ellipticity) of each of these RSV HR1 peptides at 35 μM concentration and 1 °C. As the length of the peptide increases, more helical character is adopted by the peptide in solution, as demonstrated by the two minima at 208 and 222 nm (*49*). This helicity reaches maximal levels for T-1772, T-1584, and T-1623. Calculation of the amount of helical secondary structure (see methods) results in the following helicity values: 10% (T-1590), 49% (T-1582), 69% (T-1581), 83% (T-1772), 90% (T-1584), and 88% (T-1623). The midpoints of the melting transitions (Figure 3B) also increase as the

peptide length increases: <10 °C (T-1590), 22 °C (T-1582), 31 °C (T-1581), 42 °C (T-1772), 53 °C (T-1584), and 55 °C (T-1623), indicating increased thermal stability as the peptide length increases. This increase reaches a maximum for T-1584, as no significant increase in stability is demonstrated by T-1623.

The above experiments identify T-1772 as the peptide containing the minimal sequence required for maximum helicity of the HR1 region (85−90%), while T1584 demonstrates maximum thermal stability. Despite the higher thermal stability of T-1584, we chose T-1772 to use as our HR1 model because it was easier to prepare in sufficient quantities in comparison to T1584. The size of the HR1 protected fragments in the proteinase-K experiments support the choice of HR1 model peptides in this molecular weight range.

Further examination of the thermal stability of T-1772 is presented in Figure 3C. As the concentration of T-1772 increases, the mean residue ellipticity at 222 nm increases. Therefore, the corresponding amount of helicity, as calculated from the full spectra at 1 °C (data not shown), increases: 67% (1 μM), 80% (10 μM), 83% (35 μM), 84% (50 μM), and 90% (100 μM). In addition, as the concentration of T-1772 increases, the midpoint of the thermal melting curve increases, demonstrating increased stability: 30 °C (1 μM), 32 °C (10 μM), 42 °C (50 μM), and 46 °C (100 μM). Similar concentration-dependent results are obtained for the other HR1 peptides (data not shown). The concentration dependence of the helicity and thermal stability suggest self-association of the HR1 peptide, involving helical secondary structure.

Sedimentation Equilibrium Experiments Reveal Homogeneous Self-Association of the HR1 Peptides. To further investigate self-association of the HR1 peptides, their oligomerization states were measured using analytical ultracentrifugation. Sedimentation equilibrium experiments were performed on 35 μM samples at rotor speeds of 25K, 30K, and 35K rpm. The data were fit using a single ideal species model to determine a weight-averaged molecular weight (M_w) for each sample. Homogeneity of each sample was demonstrated by the constant M_w obtained at the different rotor speeds (data not shown). The resulting M_w listed in Table 1 are averages of results obtained from three independent sample preparations tested at three rotor speeds. Each of the HR1 peptides give M_w values higher than that of the monomer molecular weights calculated from their sequences, ranging from 1.5 for the shortest peptide (T-1582) to 2.2 for the longest peptide (T-1623). These data suggest that a self-association is occurring; and the trend suggests that the extent of self-association is dependent on peptide length.

To further examine the self-association of the HR1 region, sedimentation equilibrium experiments were performed on T-1772, the shortest peptide demonstrating maximum helicity from the CD analysis. Two independent preparations of a range of concentrations (15, 25, 50, 75, 100, and 150 μM) were tested at a range of rotor speeds (13 500, 16 000, 17 000, 21 000, 24 000, 27 500, and 30 000 rpm). These individual data files were fit using a single ideal species model to determine a weight-averaged molecular weight for each concentration, presented in Table 2. Homogeneity of each sample was demonstrated by the constant M_w obtained at the three different rotor speeds, and by the overlapping traces on a graph of M_w vs radial concentration for the six concentrations (data not shown). The M_w shows a very slight concentration dependence, in which the 15 μM value is 7% lower than the average of M_w (calculated from the five highest concentrations), whereas the five highest concentrations are within 2% of the average. This average M_w is 2.4 times the monomer molecular weight, indicating a self-association.

This homogeneous self-association was further investigated by choosing different association models and testing them first for their ability to reproduce the individual data files. Figure 4 presents these results for 100 μM T-1772 at 24 000 rpm. Details of the calculation results are presented in the figure legend. The single ideal species model (Panel A) predicts a M_w of 12 925 and produces a fit with some systematic trend in the residuals, indicative of more than one species in solution. Of the self-association models monomer/tetramer (panel B), monomer/trimer (panel C), and monomer/dimer/tetramer (panel D), the monomer/trimer model produces random residuals over the entire concentration and speed data set. This indicates that the trimeric self-association

Table 1: Sedimentation Equilibrium Results for HR1 Peptides

HR1 peptide	monomer molecular weight[a]	weight-averaged molecular weight of 35 μM HR1 peptide (g/mol)[b]	range of χ-squared values[d]	*N*-mer[e]
T1582	4897	7521 ± 271 (4%)	1.2860×10^{-5}, 6.6022×10^{-5}	1.5
T1581	5007	9125 ± 466 (5%)	4.9958×10^{-6}, 1.1037×10^{-4}	1.8
T1772	5393	12 897 ± 398 (3%)[c]	1.8697×10^{-7}, 2.7917×10^{-5}	2.4
T1584	5506	11 703 ± 653 (6%)	9.7047×10^{-6}, 2.8735×10^{-4}	2.1
T1623	5750	12 899 ± 1225 (10%)	4.0381×10^{-5}, 2.8391×10^{-4}	2.2

[a] Molecular weight based on sequence and mass spectrometric analysis. [b] On the basis of calculations which model the solution as containing a single ideal species (see Materials and Methods). Reported are averages of nine data points: three independent solution preparations measured at rotor speeds of 25, 30, and 35K rpm. Errors are expressed as standard deviations and relative standard deviations of those nine values. [c] Value reported is a 25 μM concentration determination; see Table 3 for rotor speeds used. [d] Smallest and largest χ^2 values from the set of single ideal species fits used to produce the reported M_w. [e] Value is equal to the weight-averaged molecular weight (column 3) divided by the monomer molecular weight (column 2).

Table 2: Sedimentation Equilibrium Results for HR1 Model Peptide T-1772 vs Concentration

concentration (μM)	weight-averaged molecular weight (g/mol)[a]	range of χ-squared values[b]
15	11 915 ± 699 (6%)	9.2561×10^{-8}, 2.9123×10^{-5}
25	12 897 ± 398 (3%)	1.8697×10^{-7}, 2.7917×10^{-5}
50	12 797 ± 594 (5%)	1.4797×10^{-7}, 2.6800×10^{-5}
75	12 588 ± 369 (3%)	7.2019×10^{-4}, 4.9504×10^{-5}
100	13 036 ± 637 (5%)	3.1340×10^{-6}, 9.2988×10^{-6}
150	12 523 ± 465 (4%)	8.3774×10^{-6}, 1.6254×10^{-5}

[a] On the basis of calculations which model the solution as containing a single ideal species (see Materials and Methods). Value is an average of seven data points: one solution preparation tested at four rotor speeds (13 500, 16 000, 24 000, and 27 500 rpm) and one solution preparation tested at three rotor speeds (17 000, 21 000, 30 000 rpm). Errors are expressed as standard deviations and relative standard deviations. [b] Smallest and largest χ^2 values from the set of single ideal species fits used to produce the reported M_w.

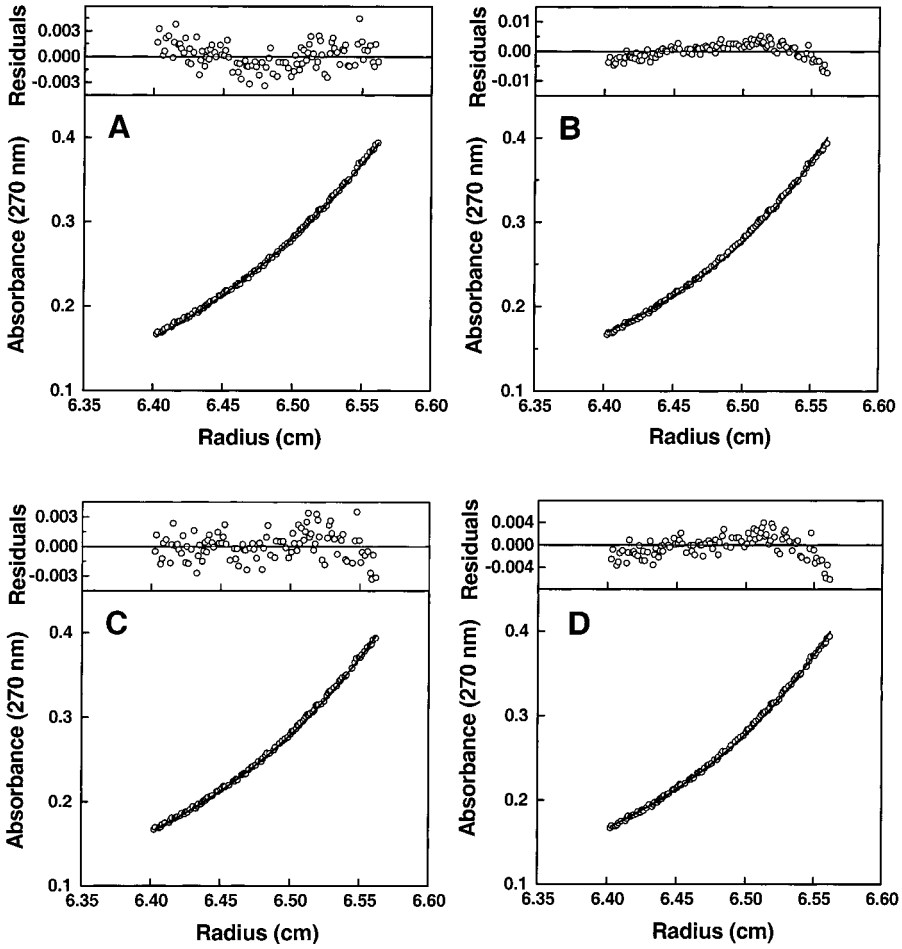

FIGURE 4: Sedimentation equilibrium data (○), representative mathematical models (superimposed solid lines) for 100 μM T-1772 in PBS pH 7 measured at 24 000 rpm, 4 °C. Residuals are displayed above each data and calculation pair. (A) Single ideal species model fit to the single data file, $M_w = 12\,925$ ($\chi^2 = 9.299 \times 10^{-6}$). (B) Self-association model fit to the single data file assuming a monomer/tetramer equilibrium, $K_a = 6.95 \times 10^{12}$ M^{-3} ($\chi^2 = 6.766 \times 10^{-6}$). (C) Self-association model fit to the single data file assuming a monomer/trimer equilibrium, $K_a = 2.45 \times 10^9$ M^{-2} ($\chi^2 = 2.015 \times 10^{-6}$). (D) Self-association model fit to the single data file assuming a monomer/dimer/tetramer equilibrium, $K_{a12} = 2.47 \times 10^4$ M^{-1}, $K_{a14} = 3.72 \times 10^{13}$ M^{-3} ($\chi^2 = 4.12 \times 10^{-6}$).

best reproduces the data and was therefore examined in more detail.

A global fit of multiple data files was then performed, using a monomer/trimer equilibrium. The data set was divided into two groups of nine files each: group 1 contained 15, 50, and 100 μM at 16 000, 24 000, and 27 500 rpm; group 2 contained 25, 75, and 150 μM at 16 000, 24 000, and 27 500 rpm. The calculation was performed by first holding the baseline offset for each file constant at zero, while allowing the association constant to vary. After this minimum was found, the association constant and each file's baseline offset were allowed to vary. Figure 5 presents the 100 μM T-1772 at 24 000 rpm data and the resulting fit. The random residuals for these data file and the other 17 files suggest that the monomer/trimer equilibrium is an appropriate model. Both groups of data produced virtually identical results for the association constants (K_a) and 95% confidence limits (CL): group 1 $K_a = 5.03 \times 10^8$ M^{-2} [CL = (4.16−6.10) $\times$ 10^8 M^{-2}, goodness of fit = 0.078 24); group 2 $K_a = 5.37 \times 10^8$ M^{-2} [CL = (4.49−6.71) $\times$ 10^8 M^{-2}, goodness of fit = 0.1342]. The average values are $K_a = 5.2 \times 10^8$ M^{-2}, with CL = (4.2−6.4) $\times$ 10^8 M^{-2}.

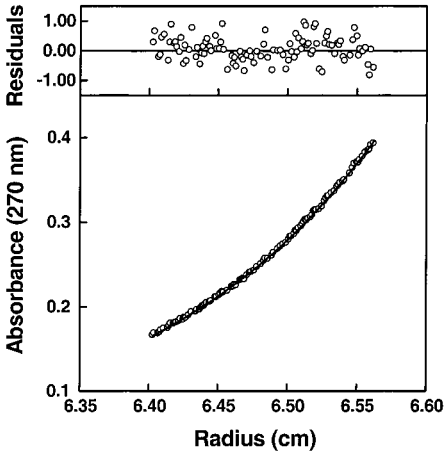

FIGURE 5: Example of the result from a global analysis of multiple data files of T-1772 in PBS pH 7 measured at 4 °C. Sedimentation equilibrium data shown is for 100 μM concentration at 24 000 rpm rotor speed. The self-association model is for a monomer/trimer equilibrium, $K_a = 5.2 \times 10^8$ M^{-2} [goodness of fit = 0.078 24; 95% confidence limit = (4.2−6.4) $\times$ 10^8 M^{-2}] See text for additional details.

Studies of HR2 Peptide Reveals Random Monomeric Secondary Structure. The HR2 peptide T-112 demonstrates little secondary structure as seen by its CD spectra at concentrations of 10 and 50 μM at 1 °C (Figure 6A). Calculations based on these spectra predict less than 10% helicity in PBS solution. In addition, CD melting curves of

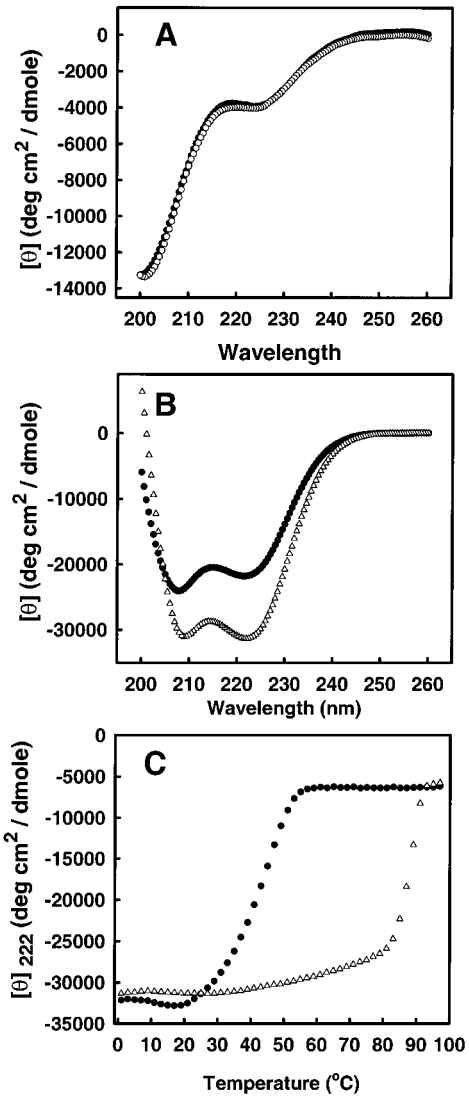

FIGURE 6: (A) Circular dichroism spectra (mean residue ellipticity) of 10 μM (●) and 50 μM (○) HR2 peptide T-112. (B) Circular dichroism spectra for mixtures of T-1772 and T112, comparing the model for no interaction (●, see text) with the experimental spectrum of a mixture of 50 μM T-1772 and 50 μM T-112 (△). (C) Mean residue ellipticity as a function of temperature compared for 50 μM T-1772 (●) and a mixture of 50 μM T-1772 and 50 μM T-112 (△).

10 and 50 μM solutions reveal little thermal stability, independent of concentration (data not shown). Sedimentation equilibrium studies of 50 μM samples of T-112 at 25 000, 30 000, and 35 000 rpm results in a M_w of 3984 (data not shown); comparison to the molecular weight based on the peptide sequence (4030) demonstrates that T-112 behaves as a monomer in solution.

CD Studies of HR1−HR2 Peptide Mixtures Reveal an Increase in Helicity upon Interaction. To probe the interaction of the HR2 peptide T-112 with the HR1 peptide T-1772, the CD spectra of mixtures of these peptides were compared to a model for no structural change upon interaction (see Materials and Methods). Figure 6 presents the CD spectra (panel B) and thermal stability results (panel C) for an equimolar mixture (50 + 50 μM) of the two peptides. The 1 °C spectrum of the mixture of the peptides (△) is markedly different than the model for no structural change upon interaction (●). Indeed, the helicity value of the mixture (86%) is greater than that which would be present if no interaction occurred (55%). This demonstrates that an increase in helicity of the peptides in solution results from their interaction. The thermal stability (panel C) of the HR1−HR2 mixture (T_m = 87 °C, △) is much greater than that of the HR1 peptide alone (42 °C, ●). Thus, the interaction of HR1−HR2 produces an extremely stable, helical moiety.

Table 3: Sedimentation Equilibrium Results for Mixtures of the HR1 Peptide T-1772 and the HR2 Peptide T-112

T-1772 concentration (μM)	T-112 concentration (μM)	weight-averaged molecular weight (g/mol)[a]	range of χ^2-squared values[b]
50	10	15 269 ± 649 (4%)	1.4774×10^{-6}, 1.4195×10^{-4}
50	50	22 021 ± 1050 (5%)	6.7290×10^{-6}, 1.2966×10^{-4}
50	100	17 282 ± 1396 (8%)	1.5072×10^{-5}, 8.1949×10^{-4}

[a] On the basis of calculations which model the solution as containing a single ideal species (see Materials and Methods). Value is an average of seven data points: one solution preparation tested at four rotor speeds (13 500, 16 000, 24 000, 27 500 rpm) and one solution preparation tested at three rotor speeds (17 000, 21 000, 30 000 rpm). Errors are expressed as standard deviations and relative standard deviations. [b] Smallest and largest χ^2 values from the set of single ideal species fits used to produce the reported M_w.

Sedimentation Equilibrium Experiments Reveal Hexameric Oligomerization State of the HR1−HR2 Interaction Pair. To investigate the oligomerization state of the HR1−HR2 peptides, sedimentation equilibrium experiments were performed on two independent sample preparations of different ratios of the peptides T-1772 and T-112: 50 + 10 μM; 50 + 50 μM; and 50 + 100 μM, respectively. These samples were run at seven rotor speeds: 13 500, 16 000, 17 000, 21 000, 24 000, 27 500, and 30 000 rpm. Table 3 presents the results of fitting these data to a single ideal species model to obtain a weight-averaged molecular weight. The M_w value reaches a maximum for the sample containing equimolar concentrations of 50 μM for each peptide, suggesting a 1:1 stoichiometry of the interaction. Diagnostic graphs of M_w/M_{w0} vs rpm/rpm$_0$ for the 50 + 10 and 50 + 50 μM mixtures indicate a homogeneous association (data not shown). Panel A of Figure 7 presents the single ideal species fit of the 27 500 rpm data. Two factors suggest that this is not an appropriate model. First, the systematic pattern of residuals indicates that it is unlikely that only one species is present in solution. Second, the average molecular weight is 22 021, which approaches but does not precisely correspond to an even multiple of the monomeric molecular weights of the HR1 and HR2 peptides (20% lower than a species which contains three of each peptide = 28 269).

Since it is possible that the hetero-complex is not fully formed at these concentrations, another modeling approach was considered. This approach takes into consideration that small amounts of unassociated HR1 and HR2 peptides could be present in solution. For simplicity, our approach to modeling these data simply added a second ideal species to the original model. We tested two models for the final oligomerization state of the HR1−HR2 moiety: a six-membered complex and an eight-membered complex. In both models, the second species was taken to have a molecular weight of 8400, corresponding to the average of the weight-averaged molecular weights for the individual peptides

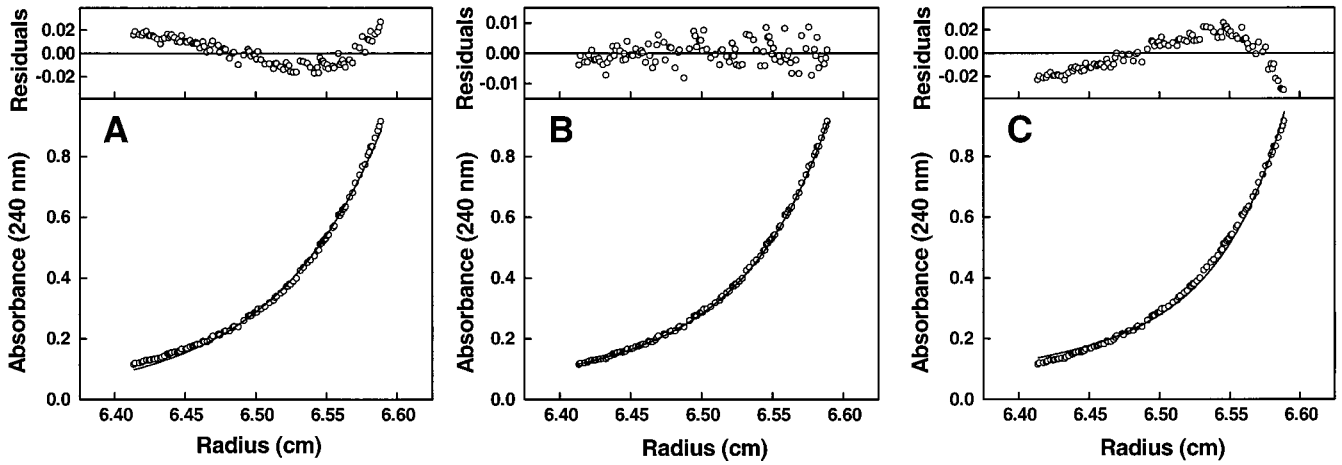

FIGURE 7: Sedimentation equilibrium results for a mixture of 50 μM T-1772 and 50 μM T-112, 27 500 rpm, 4 °C. (A) Single ideal species model, $M_w = 21\,097$ ($\chi^2 = 1.297 \times 10^{-4}$). (B) Two-ideal species model (see text for additional details) employing $M_{w1} = 28\,269$ (three HR1 and three HR2 peptides), and $M_{w2} = 8400$; Co1 = 0.30, Co2 = 0.15 ($\chi^2 = 1.349 \times 10^{-5}$). (C) Two-ideal species model (see text for additional details) employing $M_{w1} = 37692$ (four HR1 and four HR2 peptides), and $M_{w2} = 8400$; Co1 = 0.20, Co2 = 0.23 ($\chi^2 = 2.230 \times 10^{-4}$).

measured at these concentrations (12 797 for T-1772 and 3984 for T-112). This approach is similar to that taken by Laue et al. in their examination of a heteroassociation between two proteins (*57*). In this work, the authors used a monomer/dimer equilibrium with a hypothetical monomer having a molecular weight equal to the weight-averaged molecular weight of the reacting species. In our RSV HR1/HR2 system, we have a more complicated hetero-association scheme, involving a self-association reaction for the HR1 peptide in addition to the hetero-association of apparently multiple monomers of HR1 and HR2 peptides. Therefore, we have not attempted to extract an association constant for this hetero-association, but have simply tried to assign the correct oligomerization scheme. We assume the solution contains four species: fully associated HR1/HR2 complexes, monomeric HR2 peptide, trimeric HR1 complexes, and monomeric HR1 peptide. Our simplification of this scheme is to utilize a model which contains two ideal species: one being the fully formed complex, and the other representing the average of the weight-averaged molecular weights for the HR1 and HR2 peptides, determined above.

The results of this approach are presented in panels B and C of Figure 7. Panel B presents the fit obtained taking the primary species to have a molecular weight corresponding to a six-membered complex (28 269, formed by three HR1 and three HR2 peptides). Panel C presents the fit obtained taking the primary species to have a molecular weight corresponding to an eight-membered complex (37 692, formed by four HR1 and four HR2 peptides). As can be seen by the residual plots, the trimeric complex (panel B) is clearly the best model, producing random residuals for these data and the other speeds (data not shown). The relative concentrations reported by the calculation ("loading concentrations" of species 1 and 2: Co1 = 0.30, Co2 = 0.15) predict that the six-membered complex comprises approximately 70% of the solution species, and the remaining 30% is a mixture of unassociated HR1 and HR2 peptides.

DISCUSSION

Length of the HR1 and HR2 Domains. The protease digestion experiments of mixtures of the RSV−F_1 protein constructs and the HR2 peptide provide a valuable starting point for the identification of the HR1−HR2 interaction core. Digests of the MF−II or MF−III mixed with the HR2-peptide identify the F_1 HR1 region required for adoption of a structure resistant to proteinase-K digestion. The slightly larger protected band observed in the MF−IV + HR2 peptide digestion indicates that the HR1-protected region extends beyond the C-terminus of MF−III. Detailed studies of the synthetic peptides prepared in light of these results allow for a more rigorous identification of specific residues responsible for stabilizing the secondary structure and oligomerization of this region.

Our choice of concentrating on the binding of the HR2 peptide T-112 is based on several lines of evidence. Lambert et al. reported antiviral results from a 35-residue peptide "walk" through the putative HR2 domain (*34*). The results suggested that optimal antiviral activity was associated with the T-112 peptide and overlapping peptides extending four residues N-terminal and seven residues C-terminal to T-112. Significant loss of anti-viral potency was associated with peptides further removed from the T-112 sequence. These studies suggest that the T-112 sequence is centrally located in the biologically "active" region of HR2, and that the HR2 region in the context of the viral protein could extend beyond the 35-residue model peptide employed here. However, since the peptides shifted by five and seven residues to the N- and C-termini, respectively, do not protect the HR1 model proteins from enzymatic digestion, it is likely that T-112 contains the most energetically important contact points for this interaction. This hypothesis is also supported by preliminary work using alanine-scanning methodology.

HR1 Model Peptides. Studies of the HR1 peptides reveal interesting aspects of the sequences and structures involved in the self-association of this region of the protein. First, the CD spectra demonstrate dramatic increases in helicity as additional residues of the HR1 region are included in the synthetic peptide model. For example, adding two residues to T-1590 to make T-1582 produces an increase from 10 to 49% helicity. Adding another residue to T-1582 to make T-1581 produces another increase from 49 to 69% helicity. Last, adding four residues to the amino terminus of T-1581

to make T-1772 causes a further increase from 69 to 83%, an almost fully helical peptide. The further sequence additions that define T-1584 and T-1623 also adopt fully helical structure. These results could suggest that the DKQ and AVSK sequences that lead to the dramatic changes are responsible for the helical self-association of this protein region. However, studies of 35-residue peptides derived from this region which contain these sequences are primarily random in solution (M.K. Delmedico, and G. Merutka, unpublished). Therefore, these two sequences are important but not individually sufficient for helical self-association of this protein region. The development of secondary structure is critically dependent on the length of the peptide.

The weight-averaged molecular weight of the HR1 peptides as measured by sedimentation equilibrium increases as the model peptides lengthen, mirroring the helical increases observed in the CD spectra. The additions of one residue to T1582 to make T1581 and then four residues to make T-1772 generate modest increases in the weight-averaged molecular weight (see Table 1); these are the same sequence changes which are responsible for dramatic secondary structure changes. The peptides T-1772, T-1584, and T-1623 demonstrate approximately the same extent of self-association as evidenced by their weight-averaged molecular weight, and these peptides also display nearly identical secondary structure.

The CD spectra of T-1772 reflect a modest change in secondary structure with concentration. As the concentration increases from 1 to 10 to 100 μM, the helicity content increases from 67 to 80 to 90%, indicative of a self-association. The weight-averaged molecular weight of this peptide determined by sedimentation equilibrium remains approximately the same in the concentration range of 25−150 μM. However, the sample at the lowest concentration of T-1772 observable with our absorbance optics, 15 μM, demonstrates a slightly lower M_w than those of the other five concentrations, consistent with a self-associating complex. Thus, the small overlap in concentration ranges detectable by both CD and sedimentation equilibrium produces consistent results. Due to sample limitations, we were unable to increase the concentration in these experiments beyond 150 μM to measure the fully associated complex, but the data set obtained and analyzed herein clearly demonstrates the adoption of a monomer/trimer self-association reaction by the HR1 peptide.

Interaction of the HR1−HR2 Regions. We have identified the primary and secondary structures and oligomerization state involved in a stable association of two regions of the RSV−F_1 protein. The CD and sedimentation equilibrium results have demonstrated that the HR2 peptide T-112 adopts a random, monomeric conformation by itself in solution, while the HR1 peptide T-1772 exhibits a highly helical, trimeric self-association. Mixing the two peptides together results in greater helicity than predicted by the sum of the individual spectra, indicating that a structural change results upon interaction of these two peptides. This increase in helicity is most likely due to the HR2 peptide adopting a more helical structure upon binding to the HR1 peptide. Thermal stability studies on the complex indicate that it is a highly stable species with a $T_m = 87$ °C. Similar experiments on mixtures of the other HR1 peptides reported in this study (T-1590, T-1582, T-1581, T-1584, and T-1623) with the HR2 peptide T-112 result in identical T_m values for the complexes (R. Sen, and M.K. Delmedico, unpublished data). Since the thermal stability of these HR1 peptides (ranging from 43 to 54 residues) are dependent on the peptide length (Figure 3B), the stability of the HR1−HR2 complexes appears uniquely dependent on the presence of the HR2 peptide.

Sedimentation equilibrium results for the peptide mixtures confirm that an interaction does occur upon mixing the HR1−HR2 peptides, as evidenced from the higher molecular weight observed for the complex. The results from mixing different ratios of the two peptides strongly suggest that the stoichiometry of the complex is 1:1. Mathematical fitting of these results with a model incorporating two ideal species demonstrates that the best model for the interaction complex is a six-membered bundle containing three HR1 and three HR2 peptides. Requirement for a small amount of unassociated peptide in the model suggests that the mixtures are not fully associated at the concentrations analyzed. Presumably, higher concentrations would shift the association to a more fully associated complex.

Model for the RSV HR1−HR2 Core. Our data are consistent with a six-membered helical bundle with a 1:1 ratio of HR1 and HR2 peptides. The evidence that the HR1 peptide independently exhibits a monomer/trimer equilibrium leads to the most likely geometry for a six-membered complex being established by three HR1 peptides forming an inner trimeric helical core and three HR2 peptides coiling along the grooves of the HR1 trimer. Our data does not address the respective orientation of the HR1 and HR2 helices. By analogy to the crystallographic results on the fusion proteins of the paramyxovirus SV5 and other viruses (*12*−*15*, *17*, *19*, *20*, *23*) it is probable that these helices also adopt an antiparallel arrangement. This six-membered geometry has been demonstrated by crystallographic studies of similar regions of the fusogenic proteins from other viruses (*9*, *12*−*15*, *17*, *19*, *20*, *23*). Another similarity to other studies is found in the extreme stability of the HR1−HR2 complex. The HIV core has a T_m of 90 °C, SIV has a $T_m > 90$ °C, Ebola has a T_m of 90 °C, and SV5 has a $T_m > 90$ °C (*11*, *18*, *19*, *22*). Although participation in other stages of fusion protein structure and dynamics cannot be eliminated, the high thermal stabilities of the HR1−HR2 core structures suggests that these six-membered helical bundles are parts of the final, fusogenic states of the proteins.

Other indirect evidence for the participation of the HR1−HR2 core in the fusogenic state comes from studies which demonstrate that peptides derived from the HR2 region of RSV, HIV, HPIV-2, HPIV-3, FIV, NDV, and Sendai virus are potent, specific inhibitors of viral fusion (*31*−*38*, *58*). As shown in HIV (*44*), these HR2 peptides likely target the HR1 region in halting the function of the fusion protein. This is suggestive that at some stage of the transition from native to fusogenic states, the HR1 core must be formed without association of the HR2 region, so that the HR2 peptides can bind and prevent further conformational changes. It is difficult to predict whether the native states of fusion proteins contain a trimeric HR1 core. Further studies are needed to address these issues. Another interesting question specific to the RSV fusion mechanism relates to the role of a third heptad-repeat motif (HR3) located on the F_2 subunit, whose structure and function remains obscure. Also not established

is the structure and function of the ~250 residues which lie between the HR1 and HR2 domains.

Summary and Prospects. Like fusogenic proteins on other enveloped viruses, the RSV−F_1 protein exhibits a specific association of two heptad-repeat regions, one proximal to the fusion peptide (HR1) and one proximal to the membrane-spanning region (HR2). Our peptide studies demonstrate that this association is mediated by a trimeric coiled-coil HR1 structure to which three HR2 regions bind by adopting helical structure. The result is a very stable, helical complex containing three HR1 and three HR2 members. This work adds RSV to the growing group of viral fusion proteins which contain this six-membered helical bundle.

For the HIV system, we previously correlated the antiviral activity of HR2-derived peptides with their ability to bind to an HR1 target in solution (*41*). One of these peptides, T-20, is showing efficacy in Phase II clinical trials, and is the first viral fusion inhibitor to be tested in humans (*45*, *59*). This demonstrates the proof of concept that preventing the activity of the viral fusion protein is a viable target for therapeutic intervention. We are exploiting this approach to the discovery of antiviral compounds for a variety of enveloped viruses, including RSV.

NOTE ADDED IN PROOF

During the review process of this article, a related paper on the HR1−HR2 interactions of the RSV fusion protein of subgroup B, strain 18537 appeared (*60*). There are several differences between the two studies: (1) A much greater increase in helicity as a result of HR1−HR2 binding is observed herein (30% increase) than observed in the other study (7% increase); (2) The HR1 association constant obtained herein (5.2×10^8 M^{-2}) is lower than that obtained in the other study (2.2×10^{11} M^{-2}); and (3) The HR1−HR2 complex is ~70% formed at the concentrations used herein, whereas the other study reports a molecular weight close to that corresponding to a fully-formed six-membered complex, following purification over an analytical gel filtration column (unreported final concentrations). Some of these differences may be due to differences in the peptide models employed. In particular, the lengths of the peptides differ. As demonstrated by our data, the secondary structure and self-association behavior of the HR1 model peptides are length dependent. Also, there are four HR1 residues and three HR2 residues that differ between subgroup A and B viruses for the overlapping HR1 and HR2 peptide sequences. Despite these differences, similar conclusions are reached regarding the stoichiometry and secondary structure of the RSV HR1−HR2 core.

ACKNOWLEDGMENT

The authors thank Drs. Dani Bolognesi, Michael A. Mink, Peter W. Jeffs, and Joel Erickson for their support of this project.

REFERENCES

1. McIntosh, K., and Chanock, R. M. (1990) in *Virology* (Fields, B. N., and Knipe, D. M., Eds.) pp 1045−1072, Raven Press, Ltd., New York.
2. Toms, G. (1994) *Virus Life January*, 2−5.
3. Morrison, T. G. (1988) *Virus Res. 10*, 113−136.
4. Levine, S., Klaiber-Franco, R., and Paradiso, P. R. (1987) *J. Gen. Virol. 68*, 2521−2524.
5. White, J. M. (1992) *Science 258*, 917−924.
6. Hernandez, L. D., Hoffman, L. R., Wolfsberg, T. G., and White, J. M. (1996) *Annu. Rev. Cell Dev. Biol. 12*, 627−661.
7. Lamb, R. A. (1993) *Virology 197*, 1−11.
8. Carr, C. M., and Kim, P. S. (1993) *Cell 73*, 823−832.
9. Wilson, I. A., Skehel, J. J., and Wiley, D. C. (1981) *Nature 289*, 366−373.
10. Bullough, P. A., Hughson, F. M., Skehel, J. J., and Wiley, D. C. (1994) *Nature 371*, 37−43.
11. Lu, M., Blacklow, S. C., and Kim, P. S. (1995) *Nat. Struct. Biol. 2*, 1075−1082.
12. Chan, D. C., Fass, D., Berger, J. M., and Kim, P. S. (1997) *Cell 89*, 263−273.
13. Weissenhorn, W., Dessen, A., Harrison, S. C., Skehel, J. J., and Wiley, D. C. (1997) *Nature 387*, 426−430.
14. Tan, K., Liu, J.-H., Wang, J.-H., Shen, S., and Lu, M. (1997) *Proc. Natl. Acad. Sci. U.S.A. 94*, 12303−12308.
15. Malashkevich, V. N., Chan, D. C., Chutkowski, C. T., and Kim, P. S. (1998) *Proc. Natl. Acad. Sci. U.S.A. 95*, 9134−9139.
16. Caffrey, M., Cai, M., Kaufman, J., Stahl, S. J., Wingfield, P. T., Covell, D. G., Gronenborn, A. M., and Clore, G. M. (1998) *EMBO J. 17*, 4572−4584.
17. Yang, Z.-N., Mueser, T. C., Kaufman, J., Stahl, S. J., Wingfield, P. T., and Hyde, C. C. (1999) *J. Struct. Biol. 126*, 131−144.
18. Ji, H., Bracken, C., and Lu, M. (2000) *Biochemistry 39*, 676−685.
19. Weissenhorn, W., Calder, L. J., Wharton, S. A., Skehel, J. J., and Wiley, D. C. (1998) *Proc. Natl. Acad. Sci. U.S.A. 95*, 6032−6036.
20. Malashkevich, V. N., Schneider, B. J., McNally, M. L., Milhollen, M. A., Pang, J. X., and Kim, P. S. (1999) *Proc. Natl. Acad. Sci. U.S.A. 96*, 2662−2667.
21. Fass, D., Harrison, S. C., and Kim, P. S. (1996) *Nat. Struct. Biol. 3*, 465−469.
22. Joshi, S. B., Dutch, R. E., and Lamb, R. A. (1998) *Virology 248*, 20−34.
23. Baker, K. A., Dutch, R. E., Lamb, R. A., and Jardetzky, T. S. (1999) *Mol. Cell 3*, 309−319.
24. Gallaher, W. R., Ball, J. M., Garry, R. F., Griffin, M. C., and Montelaro, R. C. (1989) *AIDS Res. Hum. Retroviruses 5*, 431−440.
25. Chambers, P., Pringle, C. R., and Easton, A. J. (1990) *J. Gen. Virol. 71*, 3075−3080.
26. Gallaher, W. R. (1996) *Cell 85*, 1−2.
27. Buckland, R., and Wild, F. (1989) *Nature 338*, 547-.
28. Delwart, E. L., Mosialos, G., and Gilmore, T. (1990) *AIDS Res. Hum. Retroviruses 6*, 703−706.
29. Cohen, C., and Parry, D. A. D. (1986) *Trends Biochem. Sci. 11*, 245−248.
30. O'Shea, E. K., Klemm, J. D., Kim, P. S., and Alber, T. (1991) *Science 254*, 539−544.
31. Wild, C., Oas, T., McDanal, C., Bolognesi, D., and Matthews, T. (1992) *Proc. Natl. Acad. Sci. U.S.A. 89*, 10537−10541.
32. Wild, C., Greenwell, T., and Matthews, T. (1993) *AIDS Res. Hum. Retroviruses 9*, 1051−1053.
33. Wild, C. T., Shugars, D. C., Greenwell, T. K., McDanal, C. B., and Matthews, T. J. (1994) *Proc. Natl. Acad. Sci. U.S.A. 91*, 9770−9774.
34. Lambert, D. M., Barney, S., Lambert, A. L., Guthrie, K., Medinas, R., Davis-Rhodes, D. E., Bucy, T., Erickson, J., Merutka, G., Matthews, T. J., and Petteway, J., S. R. (1996) *Proc. Natl. Acad. Sci. U.S.A. 93*, 2186−2191.
35. Yao, Q., and Compans, R. W. (1996) *Virology 223*, 103−112.
36. Lombardi, S., Massi, C., Indino, E., La Rosa, C., Mazzetti, P., Falcone, M. L., Rovero, P., Fissi, A., Pieroni, O., Bandecchi, P., Esposito, F., Tozzini, F., Bendinelli, M., and Garzelli, C. (1996) *Virology 220*, 274−284.
37. Young, J. K., Hicks, R. P., Wright, G. E., and Morrison, T. G. (1997) *Virology 238*, 291−304.

38. Ghosh, J. K., Ovadia, M., and Shai, Y. (1997) *Biochemistry 36*, 15451−15462.
39. Chen, C.-H., Matthews, T. J., McDanal, C. B., Bolognesi, D. P., and Greenberg, M. L. (1995) *J. Virol. 69*, 3771−3777.
40. Wild, C., Greenwell, T., Shugars, D., Rimsky-Clarke, L., and Matthews, T. (1995) *AIDS Res. Hum. Retroviruses 11*, 323−325.
41. Lawless, M. K., Barney, S., Guthrie, K. I., Bucy, T. B., Petteway, S. R., Jr., and Merutka, G. (1996) *Biochemistry 35*, 13697−13708.
42. Matthews, T. J., Wild, C., Chen, C.-h., Bolognesi, D. P., and Greenberg, M. L. (1994) *Immunol. Rev.* 93−104.
43. Young, J. K., Li, D., Abramowitz, M. C., and Morrison, T. G. (1999) *J. Virol. 73*, 5945−5956.
44. Rimsky, L. T., Shugars, D. C., and Matthews, T. J. (1998) *J. Virol. 72*, 986−993.
45. Kilby, J. M., Hopkins, S., Venetta, T. M., DiMassimo, B., Cloud, G. A., Lee, J. Y., Alldredge, L., Hunter, E., Lambert, D., Bolognesi, D., Matthews, T., Johnson, M. R., Nowak, M. A., Shaw, G. M., and Saag, M. S. (1998) *Nat. Med. 4*, 1302−1307.
46. Olmsted, R. A., and Elango, N. (1986) *Proc. Natl. Acad.Sci. U.S.A. 83*, 7462−7466.
47. Fields, G. B., and Noble, R. L. (1990) *Int. J. Pept. Protein Res. 35*, 161−214.
48. King, D. S., Fields, C. G., and Fields, G. B. (1990) *Int. J. Pept. Protein Res. 36*, 255−266.
49. Cantor, C. R., and Schimmel, P. R. (1980) *Biophysical Chemistry Part II: Techniques for the Study of Biological Structure and Function*, W. H. Freeman and Company, New York.
50. Johnson, J., and Curits, W. (1990) *Proteins: Struct., Funct., Genet. 7*, 205−214.
51. Laue, T. M., Shah, B. D., Ridgeway, T. M., and Pelletier, S. L. (1992) in *Analytical Ultracentrifugation in Biochemistry and Polymer Science* (Harding, S. E., Rowe, A. J., and Horton, J. C., Eds.) pp 90−125, Royal Society of Chemistry, Cambridge.
52. Laue, T. M. (1992) Beckman Instruments, Inc., Spinco Business Unit, Palo Alto, CA.
53. McRorie, D. K., and Voelker, P. J. (1993) *Self-Associating Systems in the Analytical Ultracentrifuge*, Beckman Instruments, Inc., Palo Alto.
54. Yphantis, D. A., Correia, J. J., Johnson, M. L., and Wu, G.-M. (1978) in *Physical aspects of protein interactions: proceedings of the Symposium on Protein Interactions, American Chemical Society meeting* (Catsimpoolas, Ed.) pp 275−303, Elsevier, Miami Beach, FL.
55. Johnson, M. L., and Straume, M. (1994) in *Modern Analytical Ultracentrifugation* (Schuster, T. M., and Laue, T. M., Eds.) pp 37−65, Birkhauser, Boston.
56. Collins, P. L., Huang, Y. T., and Wertz, G. W. (1984) *Proc. Natl. Acad.Sci. U.S.A. 81*, 7683−7687.
57. Luckow, E. A., Lyons, D. A., Ridgeway, T. M., Esmon, C. T., and Laue, T. M. (1989) *Biochemistry 28*, 2348−2354.
58. Jiang, S., Lin, K., Strick, N., and Neurath, A. R. (1993) *Biochem. Biophys. Res. Commun. 195*, 533−538.
59. Bolognesi, D., Matthews, T., Kang, M. C., and Hopkins, S. (2000) in *7th Conference on Retroviruses and Opportunistic Infections*, San Francisco, CA.
60. Matthews, J. M., Young, T. F., Tucker, S. P., and MacKay, J. P. (2000) *J. Virol. 74*, 5911−5920.

BI000471Y